Subproject B1.9

Controlling Electron Tranport in Carbon Nanotubes and Graphene with an Optical Microresonator Cavity

Principle Investigator: Ralph Krupke

CFN-Financed Scientists: Michael Engel (3/4 BAT IIa, 28 months)

Further Scientists: Dr. Frank Hennrich (C3.4), Dr. Mathias Steiner (IBM Yorktown Heights)

Physikalisches Institut
Karlsruher Institut für Technologie

Institut für Nanotechnologie
Karlsruher Institut für Technologie

Controlling Electron Tranport in Carbon Nanotubes and Graphene with an Optical Microresonator Cavity

Introduction and Summary

Carbon nanotubes (CNT) and graphene are novel materials with great promise for future electronic, optical, and optoelectronic applications. Gaining fundamental understanding of the underlying physics in these materials is very important for any technology that may arise. In particular a better understanding of the interaction of light with low-dimensional matter is essential.
CNT and graphene exhibit unique optical and electronic properties owing to their peculiar atomic structure and dimensionality [1,2]. For example metallic CNTs and graphene combine low optical absorption with high electrical conductivity in a unique way, which makes them superior to ITO and hence likely to be applied as transparent and conductive coatings [2]. However this kind of passive-device application should only mark the beginning of an exciting development. Certainly, the great potential of those materials will be revealed once CNTs and graphene get integrated as active components in truly nanoscale optoelectronic devices, such as electro-optic modulator, photodetectors, sensors, and emitters. This development has started very recently and is the major guideline along which research is conducted in this subproject [3,4,B1.9:8].

In detail we study in subproject B1.9 the light-matter interaction by tuning the photonic environment of carbon nanotube and graphene electronic devices. Our approach has thereby been to integrate functional CNT and graphene devices into an optical microresonator cavity. In such a cavity the confinement of light in one or more dimensions alters the photonic density of states dramatically as compared to the free space. This can have severe consequences for a material which interacts with light inside a cavity, i.e. one may observe enhanced or inhibited absorption or emission depending on whether the optical transition is allowed or not, which is entirely determined by the cavity [5]. A recent example with CNT's is the experimental work by Xia et al. [6], where the electroluminescence of a semiconducting CNT has been coupled to a planar microcavity. The experiment shows that the emission linewidth is considerably narrowed compared to the free space experiment and thereby demonstrates an important aspect of cavity physics, i.e. spectral narrowing.
In our experiments the integration of devices in microcavities was motivated by the idea to populate or to depopulate non-equilibrium phonons in metallic carbon nanotubes and thereby to control the high-bias conductance in CNT devices [7]. This requires to control Raman scattering cross-sections within the cavity, e.g. reducing or enhancing anti-Stokes Raman transitions, via tuning of the photonic resonance condition.
But before such experiments can be preformed, a number of technical challenges had to be resolved. The immediate integration of CNT devices into microcavities on commonly used substrates is not possible. The standard substrate in CNT and graphene device fabrication is silicon, typically capped with an oxide layer of silicon oxide (Fig.1a). Silicon is, for the wavelength range of interest, opaque impeding optical measurements in transmission. Furthermore, silicon is not suitable as an intracavity medium due to its strong absorption in the visible. Hence, we had to replace silicon with dielectric layers with weak absorption that can be fabricated with nanometer precision.
Above all, it had not been clear *a priori* what impact the process flow will have on the material properties. Even if integration of CNT devices would be successful their properties might degrade.
Within the two years of this project, we succeeded in developing a technological platform that allows the reliable integration of CNT and graphene devices into optical microcavities with well-defined properties (Fig.1b), while maintaining their favorable optical and electronic properties. This

has been achieved by a close collaboration with Dr. Frank Hennrich who provides the dispersion of sorted carbon nanotubes (C3.2) and Dr. Mathias Steiner from IBM who provides additional optical characterization methods and expertise.
Unfortunately we are not allowed to present here the experimental results on the interaction of light with the optically confined and electrically biased Graphene material, because the data is under review by the IBM patent officers on the basis of a Joint Study Agreement between KIT and IBM. Therefore we will present now the development of the technological platform with the fabrication and characterization of the cavity devices. Integrity tests on integrated CNT devices will be presented in the context with our recent results on hot-phonon generation [B1.9:1] and phonon-mediated electroluminescence[B1.9:7]. Finally we report on the fabrication of a CNT based light-emitting diode, as a nice example for the successful collaborative work with IBM [B1.9:8].

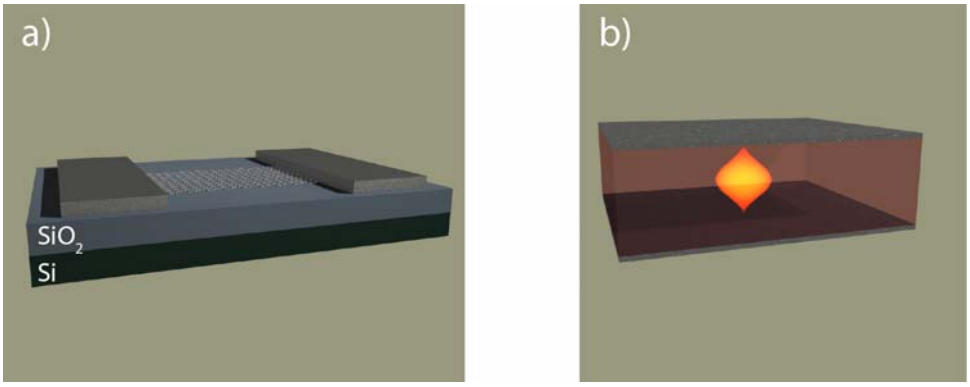

Fig.1: a) Graphene device in a conventional three terminal configuration. Two metallic electrodes make contact to the graphene which lies on top of an oxidized silicon wafer acting as a global back gate electrode separated. b) Most simple realization of an optical cavity where light is confined in one dimension between two metallic mirrors. Schematically illustrated is the intensity of the electric field of the fundamental cavity mode. The challenge of B1.9 has been to integrate a) into b) to form a device embedded in an optical cavity and to study its interaction with light.

This proof-of-concept illustrates the feasibility of integrating CNT devices into microcavities, which opens up many directions to explore like for example more efficient conversion of light in photovoltaic devices or nanoscale emitters based on CNT's.

1. Technological Platform for Device Integration

For reproducible device fabrication with high throughput we have combined the CNT processing techniques developed in the subproject C3.2 of Prof. Kappes with the dielectrophoretic assembling technique refined in this subproject B1.9. On the material side we greatly benefit from the recent advances in post-synthesis treatment of CNT in sorting by electronic type [8] and/or chirality [9], which gives access to CNT dispersions highly enriched with either metallic or semiconducting tubes. Moreover recent progress in dispersing CNT's with structure selective polymers in organic solvents even allows for dispersions of highly enriched dispersions with CNT's of a single chirality only.
The dielectrophoretic assembling technique (DEP) allows us to assemble the sorted CNT's or graphene in desired locations on the target substrate [10,B1.9:3]. Hereby, a small alternating voltage is applied between two prepatterned contacts inducing a dipole moment in the CNT leading to an attractive force that pins the CNT/graphene between the contacts. The combination of DEP with the highly separated CNT dispersions enabled us to produce very recently single-chirality CNT device arrays, which currently poses the state-of-art in CNT device fabrication[B1.9:3].

The rather large number of CNT devices makes it a challenge to identify defective devices or devices with unwanted types of CNT in an acceptable time. Therefore we have developed the voltage-contrast scanning electron microscopy method (VCSEM) as a fast characterization technique, which works very well at low magnification and electron irradiation[B1.9:2]. The influence of high irradiation dose on the device performance has been investigated in C4.1 [11].

2. Integration into an Optical Microresonator Cavity

For the integration of the CNT devices into an optical microresonator cavity, the standard silicon substrate had to be placed by a material which is suitable as an intracavity medium. We have chosen to work with silicon nitride as low loss dielectric material and prepared CNT devices on commercially available 50nm thin silicon nitride membranes, suspended over an area of 50x50micron^2 on a silicon support. The chosen thickness of 50nm Si3N4 in combination with a second intracavity medium allows for easy tuning of the cavity resonance over the visible wavelength range.
First we have prepared the CNT devices - as described before - on top of the suspended Si3N4 membranes, and wire-bonded them to a ceramic package (Fig.2a). The devices were then characterized by VCSEM and charge transport measurements (Fig.2b). Next, the second intracavity medium had to be deposited on top of the CNT devices. We have chosen to grow thin films of Al_2O_3 by the atomic layer deposition (ALD), as this process allows fabricating dielectric layers with nanometer precision. Moreover ALD-grown Al_2O_3 has excellent electrical and optical properities, e.g. low loss, high electric breakdown field, and low leakage.

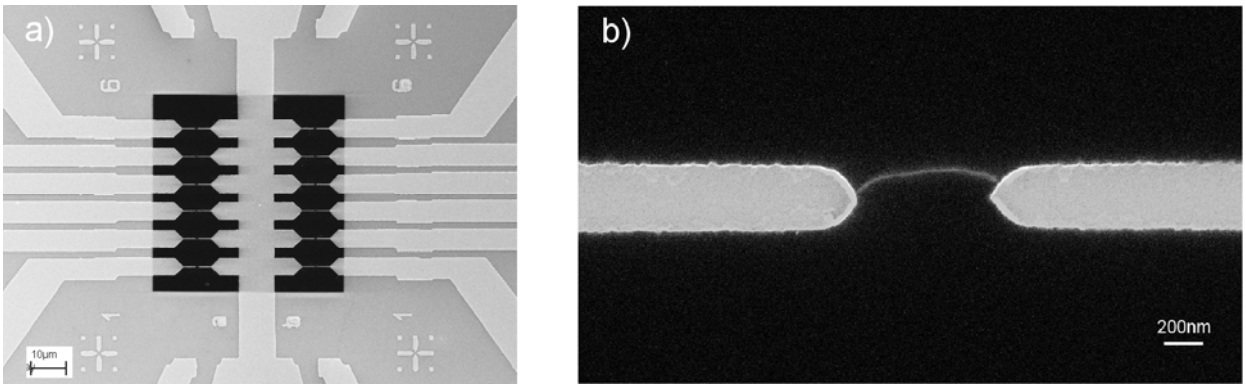

Fig.2: a) SEM image of lithographically defined metal electrodes on top of a 50nm thin Si_3N_4 membrane (dark region). b) Site-selective placement of a single metallic CNT between one electrode pair obtained by low-frequency dielectrophoresis.

The cavity resonance will be determined by the thickness of the Si_3N_4 and Al_2O_3 layers. To determine the Al_2O_3 thickness to grow, we have modeled the cavity resonance within a standard transfer matrix approach, i.e. a plane wave propagates through this multilayered cavity system and the electric field is evaluated at each boundary. From the simulations we infer the proper Al_2O_3 thickness for a targeted cavity resonance wavelength (Fig.3a). For validation of the simulations we have build test cavities without CNTs. The results shown in Fig.3b demonstrate the level of control over the cavity resonance by adjusting the alumina layer. The achieved Q factors are rather low (Fig.3c), but in agreement with other works based on planar cavities with metallic mirrors where the Q factor is limited by absorption in the metal mirrors.

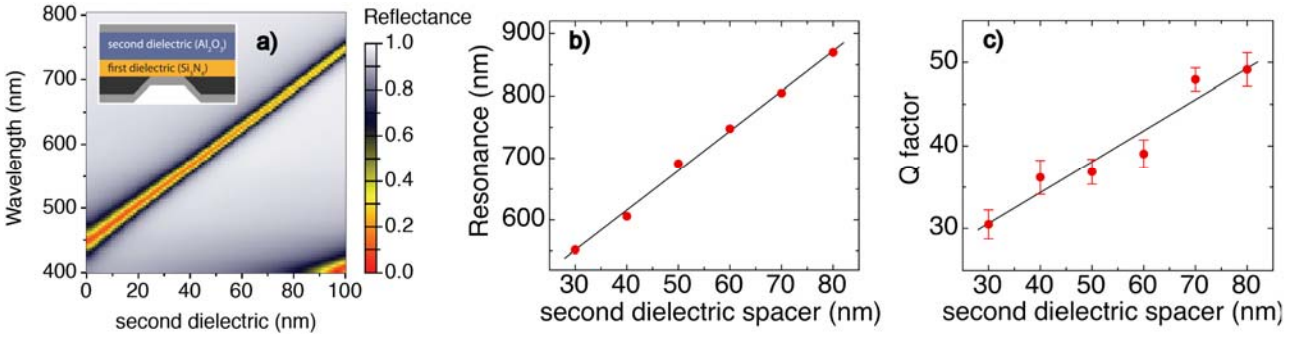

Fig.3: a) Calculated reflectance for the planar microcavity (inset) based on a transfer matrix approach, as a function of wavelength and of the dielectric spacer thickness. The sharp resonance corresponds to the fundamental cavity mode where the λ/2 condition is fulfilled. b) Resonance wavelength of the fundamental cavity mode as a function of the intracavity dielectric layer thickness and c) corresponding quality factors obtained from transmission spectra fits. Data points are average values from four cavities for each dielectric spacer thickness

For actual devices integrated into an optical microcavity the metallic mirrors needed to be defined locally, in contrast to the test cavities, the reason being that each device needs to be electrically addressed separately. Hence, another e-beam lithography step was required to locally define the cavity mirrors. As an example we show in Fig.4 a CNT thin film device prior and after microcavity fabrication.

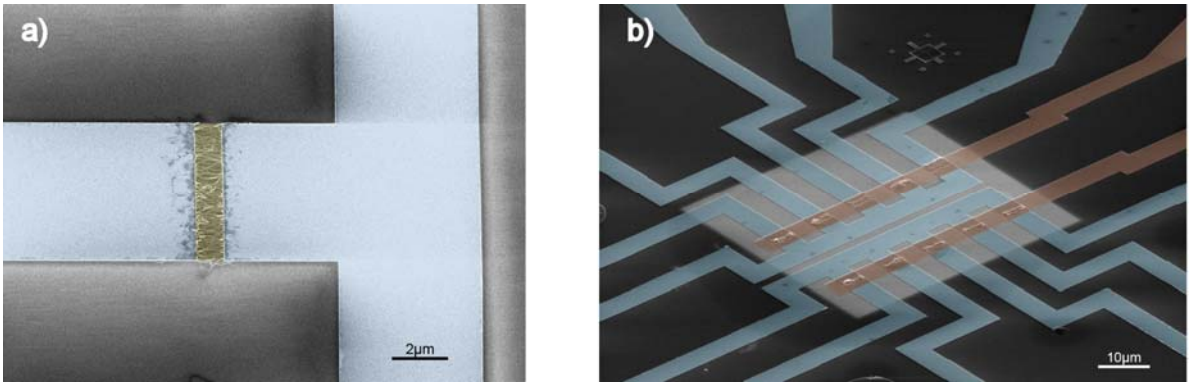

Fig.4: a) False color SEM image of an assembled CNT thin film(yellow) between metal electrodes (blue) before deposition of the intra-cavity dielectric and top metal mirror. b) Final CNT thin film device integrated into the optical microcavity.

3. Integrity test

The integrated CNT devices have to be tested for their integrity and to exclude that the process flow has an influence on the material properties. We have chosen Raman spectroscopy as a suitable characterization tool, also because we aim in B1.9 to control those phonon populations which influence the charge transport. Before we present the Raman data from the integrated devices we report here for reference on the non-equilibrium phonon populations that we have studied on CNT devices without cavity:

The motivation for measuring Raman spectra under current-bias was the early observation of current saturation under high-bias [12]. It had been suggested that electron scattering with high-energy phonons leads to an increase of the phonon occupation number and to a reduction of the electron-mean free path. Later Raman spectroscopy data supported the idea that electron-phonon coupling could be strong in carbon nanotubes [13]. In 2005 we measured a large number of individual metallic and semiconducting CNT and could show that the high-energy G mode is significantly broadened in metallic CNT compared to semiconducting CNT [14]. The data was later

confirmed by theory and shows that electron-phonon coupling is strong in individual metallic CNT [15].
Then in 2008 we measured Raman spectra of individual metallic CNTs under voltage bias to determine the phonon-mode temperatures. We succeeded in measuring the evolution of the anti-Stokes and Stokes transitions of three modes and could show that only the G-mode temperature increases with increasing voltage (Fig.5a,b) [B1.9:1]. This data has been the first spectroscopic evidence for hot-phonon generation in metallic CNTs the motivation for starting the subproject B1.9. Recently the IBM group has also measured non-equilibrium phonon populations in semiconducting CNT devices [16].
Very recently we showed that electroluminescence from metallic CNTs is mediated by high-energy phonons (Fig.5c,d) [B1.9:7], which is further evidence for the significant electron-phonon coupling in this system.

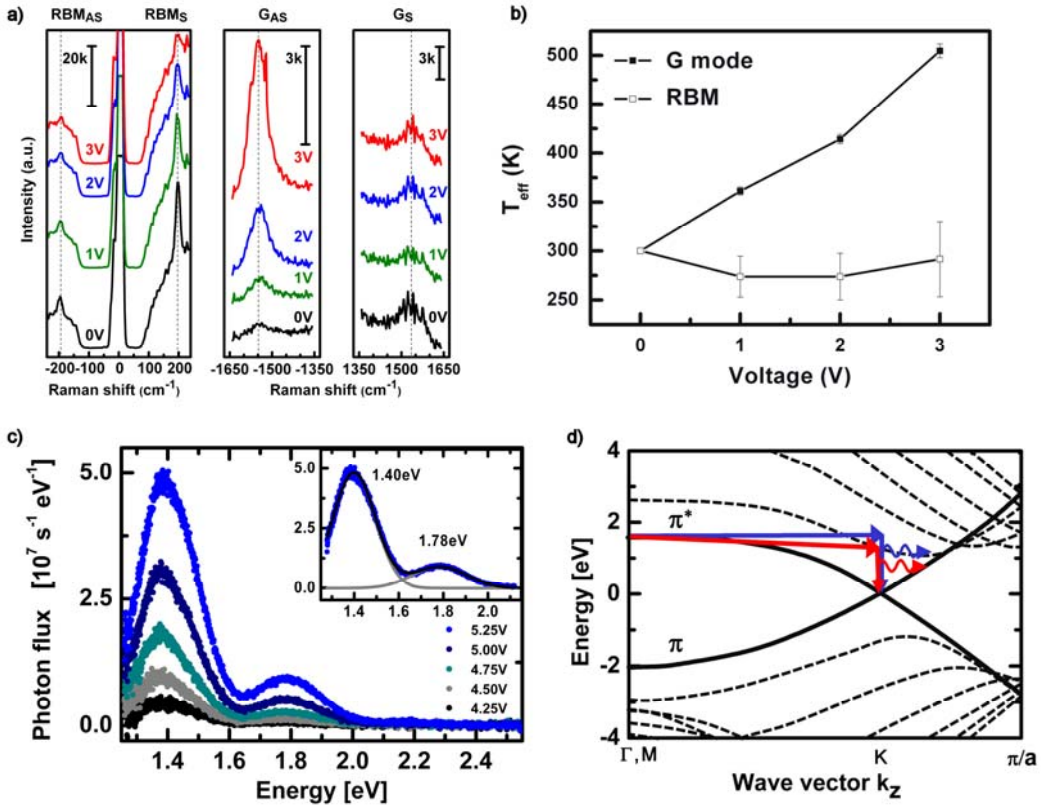

Fig.5: a-b) Raman spectroscopic evidence for hot-phonon generation in biased metallic CNTs [B1.9:1]. a) Evolution of the Stokes (S) and anti Stokes (AS) of the radial-breathing mode (RBM) and of the G mode (G) with increasing bias voltage V. b) From the spectra determined effective phonon temperatures provide evidence for non-equilibrium G-mode phonon population. c,d) Phonon-assisted electroluminescence from metallic CNTs [B1.9:7]. c) Evolution of the electroluminescence spectra of devices prepared from medium diameter (d=0.98-0.87 nm) metallic CNTs under increasing voltage bias. Insets show the Gaussian fits to the uppermost trace with the fitted peak positions. d) Electronic band structure of a armchair metallic SWNT. The double-peak structure can be explained by light emission due to phonon-assisted radiative decay from populated π^* band states at the M point to the Fermi level at the K point is indicated by the color arrows. Emission of higher (blue wavy arrow) and lower (red wavy arrow) energetic photons is mediated by the absorption (straight blue arrow) and emission (straight red arrow) of high-energy, high-momentum phonons.

We now return to the integrity test of integrated devices. We have repeated the Raman measurements under bias on CNTs encapsulated by the Si_3N_4 and Al_2O_3 dielectric and studied the radial breathing mode (RBM) and the high-energy G-mode. We observe that the G-mode temperature increases significantly with voltage whereas the RBM temperature remains rather

constant (Fig.6). This result is very important, as it shows that a CNT which is encapsulated by the Si_3N_4/Al_2O_3 dielectrics behaves similar to a CNTs on a silicon substrate. Also the Raman line shapes appear unperturbed, which is further evidence that the process flow does not deteriorate the CNT properties significantly.

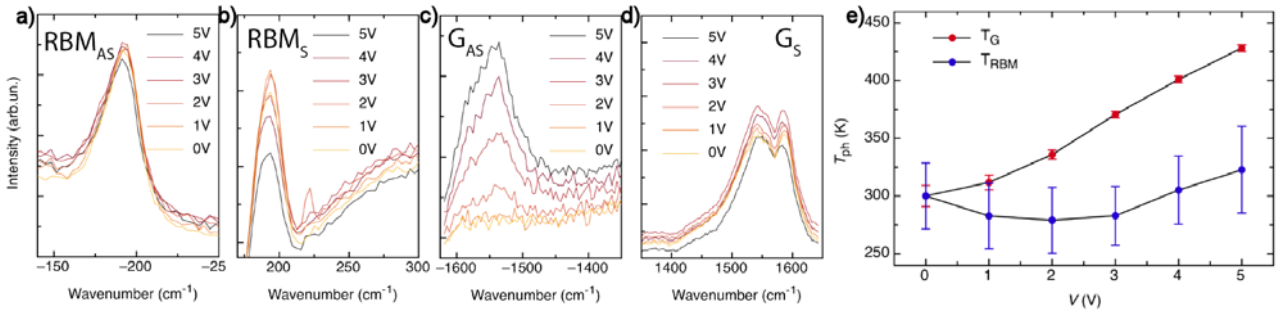

Fig.6: (a) Raman Stokes and anti-Stokes spectra of the principle phonon modes from a metallic CNT device under different voltage bias analogous to [B1.9:2]. The measured sample is an integrated device only lacking the top mirror for ease of measurement. (b) Effective phonon temperatures deduced from the data in (a). Again, a non-equilibrium phonon population is observed demonstrating that the process flow does not deteriorate the CNT properties significantly.

The concept of integrating CNTs into optical microcavities has thus been successfully implemented and we are now studying the influence of light irradiation on the transport properties of the integrated CNTs. Recently we have also integrated graphene into optical microcavities and we have studied the light emission from such devices. Unfortunately we cannot present the data because of incomplete evaluation by the IBM patent officers.

We report on a related cooperative work with IBM where we have realized a CNT thin film light emitting diode (Fig.7) [B1.9:8]. Here we have used the device integration technique presented before with the difference, that the top metal layers have been patterned to form split top gates. This way a polarized light-emitting diodes from highly aligned, separated semiconducting carbon nanotube films that show tunable light generation efficiencies and threshold-less light emission characteristics has been formed.

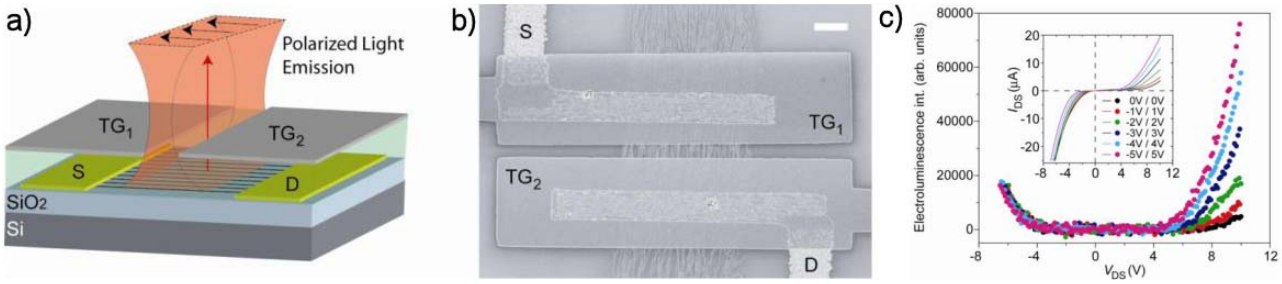

Fig.7: a) Schematic illustration and b) scanning electron microscope image of CNT film diodes with split top gates (TG_1 and TG_2). c) Electroluminescence intensity and corresponding drain-source current characteristics (inset) as a function of source-drain voltage. The associated top gate voltages V_{TG1}/V_{TG2} are denoted in the inset. Positive V_{DS} corresponds to the forward-bias direction. [B1.9:8].

References

- own work with complete titles -

[1] Ph. Avouris, Z. Chen, V. Perebeinos, Nature Photonics **2**, 341 (2008)
[2] F. Bonaccorso, F. Bonaccorso, Z. Sun, T. Hasan, A.C. Ferrari, Nature Photonics **4**, 611 (2010)
[3] F. Xia, T. Mueller, Y.-M. Lin, A. Valdes-Garcia, Ph. Avouris, Nature Nanotech **4**, 839 (2009)
[4] T. Mueller, F. Xia, Ph. Avouris, Nature Photonics **4**, 297 (2010)
[5] F. Cairo, F. De Martini, D. Murra, Phys. Rev. Lett. **70**, 1413 (1993)
[6] F. Xia, M. Steiner, Y.-M. Lin, Ph. Avouris, Nature Nanotech **3**, 609 (2008)
[7] M. Lazzeri, F. Mauri, Phys. Rev. B **73**, 165419 (2006)
[8] K. Moshammer, F. Hennrich, M.M. Kappes, Nano Res 2, 599 (2009)
[9] N. Stürzl, F. Hennrich, S. Lebedkin, M.M. Kappes, J. Phys Chem. C 113, 14628 (2009)
[10] A. Vijayaraghavan, S. Blatt, D. Weissenberger, M. Oron-Carl, F. Hennrich, D. Gerthsen, H. Hahn, R. Krupke, *Ultra-large-scale directed assembly of single-walled carbon nanotube devices.* Nano Lett. **7**, 1556 (2007)
[11] C.W. Marquardt, S. Dehm, A. Vijayaraghavan, S. Blatt, F. Hennrich, and R. Krupke, *Reversible Metal−Insulator Transitions in Metallic Single-Walled Carbon Nanotubes*, Nano Lett. 9, 2767 (2008)
[12] Z. Yao, C.L. Kane, C. Dekker., Phys. Rev. Lett. 84, 2941 (2000)
[13] M.A. Pimenta, A. Marucci, S.A. Empedocles, M.G. Bawendi, E.B. Hanlon, A.M. Rao, P.C. Eklund, R.E. Smalley, G. Dresselhaus, M.S. Dresselhaus, Phys. Rev. B **58**, R16 016 (1998)
[14] M. Oron-Carl, F. Hennrich, M.M. Kappes, H. v. Löhneysen, R. Krupke, *On the electron-phonon coupling of individual single-walled carbon nanotubes*, Nano Lett. **5**, 1761 (2005)
[15] S. Piscanec, M. Lazzeri, F. Mauri, A.C. Ferrari, J. Robertson, Phys. Rev. Lett. **93**, 185503 (2004)
[16] M. Steiner, M. Freitag, V. Perebeinos, J.C. Tsang, J.P. Small, M. Kinoshita, D. Yuan, J. Liu, Ph. Avouris, Nature Nanotech. **4**, 320 (2009)